(Received 30 June 2025, Accepted 11 August 2025, Scheduled 27 August 2025)

Performance Analysis of Breast Phantom Layers Using UWB Antenna and Dimensionality Reduction Techniques

Sonal A. Patil* and Ashwini Naik

Department of Electronics and Telecommunication Engineering, Ramrao Adik Institute of Technology, Nerul, Navi-Mumbai, India

ABSTRACT: This work explores the data-driven approaches for breast tumor detection and analysis of different breast tissues by using microwave sensing technique. Microwave sensing offers a promising trade-off in tissue penetration depth and is prominent dielectric disparity between healthy and tumorous tissues at microwave frequencies. Tumor cells exhibit unique properties, such as increased water content and different ionic compositions, which create distinct dielectric traits compared to healthy tissue. This frequently shows variations in loss characteristics compared to normal tissue and can exploit those differences for detection. The key parameter used is specific absorption rate for the determination of tumor location. The differential absorption between healthy and tumor tissues is potentially aided in identifying the presence of lesion. The five sets of reflection characteristics are recorded with the system comprising UWB antenna with breast phantom by using VNA with a gap of 4-5 days. Further, the dimensionality reduction technique is applied to extract the features using PCA and tSNE. In order to enhance the detection accuracy, dimensionality reduction techniques are used in tandem with the supervised machine learning approach. Among the four supervised algorithms, including SVM, KNN, RF, and MLP, the random forest was found to be the most optimal for the data with an auc score of 99.97%.

1. INTRODUCTION

Breast cancer, a global disease affecting mortality rates in females, is caused by gene changes, physical genetic expression, and phenotypic features. It develops in breast cells, leading to uncontrolled growth and potential fatality if not detected early. As per global statistics, breast cancer remains the second most prevalent cancer deaths, with declining survival rates requiring prompt identification for effective treatment and extended postinterventional survival. According to the National Cancer Institute and the Centers for Disease Control and Prevention, the rate of breast cancer has consistently increased, rising by 1% annually, mainly due to localized-stage and hormone receptor-positive disease. Early detection through screening and advances in treatment are the drivers of this progress. X-rays and mammograms are commonly used for diagnosing cancer; however, they have several limitations, primarily the risk of false positives and the challenges they pose for patients. There is a high chance of receiving false alarms and callbacks, resulting in expensive follow-up procedures such as biopsies. Imaging breasts with denser tissue can be particularly challenging, and not all lesions are detectable. Furthermore, patients may endure both physical and emotional discomfort during mammography, and exposure to ionizing radiation can lead to health issues. While MRI is effective for screening women with implants, it is quite costly; ultrasound is employed to monitor tumor growth and distinguish between different types of tumors [1–3]. Noninvasive methods for cancer diagnosis, including microwaves, are crucial. Microwave sensing represents a more cost-effective approach for identifying breast tumors compared to nuclear medicine and MRI, as it can eliminate the need for compressions and ionizing radiation. This technology enhances detection by identifying small lesions and anticipating the electrical properties of tissues, thereby reducing false positives and facilitating safe and comfortable diagnostic monitoring. The advancement of wireless communication and ultra-wideband (UWB) standards has necessitated high-gain broadband antennas, especially microstrip antennas, which are perfect for biomedical applications owing to their dimensions, affordability, and electrical characteristics. Research indicates that utilizing microwaves for detecting breast tumors, especially in the span of UWB, presents a favorable trade-off between the clarity of the images and the depth at which tissues can be penetrated. This method relies on the considerable variations in dielectric characteristics between healthy and cancerous breast tissues when they are examined at microwave frequencies [4]. The Federal Communication Commission (FCC) has granted the permission for emission measurement procedures in the 3.1–10.6 GHz broad frequency band, offering potential benefits for medical and communication applications [5]. A phantom is a vital scientific tool used in bio-medical research to mimic human body organs for accurate analysis and evaluation, providing reliable, quantifiable data for comparison in real-world settings. The phantoms were fabricated to be portable, facilitates rapid and precise comparisons between computer calculations for treatment planning and calculations performed manually. The research in phantom creation demonstrated that with varying compositions of the materials utilized, a significant diversity in dielectric properties

* Corresponding author: Sonal Amit Patil (sonalpatil606a@gmail.com).

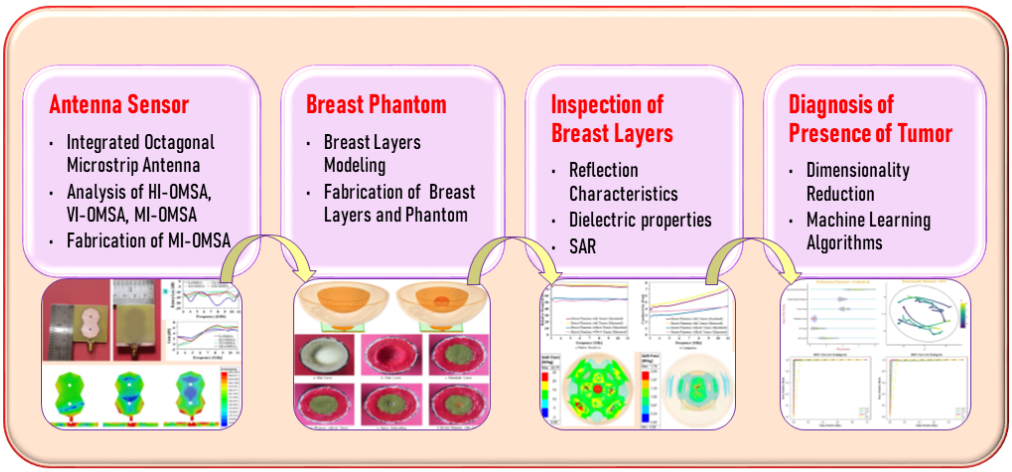

FIGURE 1. System overview.

can be achieved. The realistic 3D homogeneous and heterogeneous breast phantoms were fabricated using different materials [6–9]. The principle of microwave sensing to detect tumor depends on dielectric properties of the tissue. The dielectric traits of the tumorous region and different breast layers have significant contrasts. In order to consider these properties, the dispersion effect must be taken into account from their return losses which affect the absorption, transmission, and reflection of microwaves [10–12]. When breast tissues are exposed to electromagnetic waves, specific absorption rate (SAR) serves as a metric to quantify the amount of electromagnetic energy absorbed by tissues. SAR values were used to detect both the presence and tumor location, with lower values in the healthy than in its tumorous counterpart [13–18]. Dimensionality reduction and data visualization techniques were reported in [19–21]. Several machine learning (ML) methods were employed to improve the detection accuracy of breast tumor on Wisconsin Breast Cancer Database (WBCD). These algorithms were built on imbalanced dataset [22–26]. The detection accuracy with balanced dataset recorded by using UWB antenna was reported in [27–31]. The datasets were created by making the use of breast phantom. A solitary metasurface (MTS) Vivaldi antenna and artificial neural network (ANN) model possesses the lowest mean square error (MSE); however, it has a complicated structure and considerable large dimensions [32].

The intended objective of the proposed work is to design a system that could potentially be able to detect tumors through examination in real-time or close to real-time by utilizing breast phantom. Here, the different breast layers are analyzed by using UWB antenna reported in [33]. Further, an attempt is made to improve breast tumor detection accuracy by applying dimensionality reduction techniques on top of the supervised ML algorithms. The proposed work is organized in five sections. The system overview is described in Section 2, sensor designing in Section 3, and analysis of the breast model with its dielectric properties and SAR in Section 4. Section 5 demonstrates data analysis, dimensionality reduction techniques, and classification algorithms. The proposed system is compared with the literature in Section 6 and concluded in Section 7.

2. SYSTEM INTEGRATION

The entire proposed system incorporates four modules as illustrated in Fig. 1. In recent years, there has been a substantial surge in research related to microwave sensing, with systems requiring multiple radiating elements and complex setups, and a single antenna element that reduces size, complexity, and cost, and eliminates the need for mechanical motors. A UWB antenna sensor that has a high gain and steady radiation pattern can play a vital role in improving system sensing capability. Here, an octagon-shaped UWB antenna is employed as a sensing device for recording and inspecting the loss characteristics over the frequency span of 3.1–10.6 GHz. Breast replica is useful to analyze different breast tissues. Here, breast phantom is created to replicate the real breast characteristics. Breast tissues are examined using UWB antenna. The dielectric characteristics of the tissue serve as a framework for the microwave sensing method used to identify breast lesion. Microwave sensing of biological tissue renders its electrical characteristics, determining the levels of energy that are reflected and transmitted. Dielectric characteristics are used to realize the spatial distribution of absorbed power. The amount of power absorbed and the dielectric characteristics of both malignant and healthy cells as a function of microwave frequency are conceivable to identify presence of the tumor. A fascinating way to significantly reduce the time spent on simulations involves trial and error simulations by parameter optimization to meet expected design requirements is to use machine learning approach. Here, unsupervised and supervised techniques are used to enhance detection accuracy.

3. ANTENNA DESIGN

3.1. Antenna Geometry and Design Details

The simple octagonal shape microstrip patch antenna is designed using FR-4 epoxy, which has dielectric properties such as a substrate that is 1.59 mm thick, ε_r of 4.4, and $\tan\delta$ of 0.02. The electromagnetic waves generated through radiating element fringe off patch into the substrate. These waves radiate

into the air after being reflected from the ground surface. Radiation arises because of this fringing field that exists between the patch and the ground. The dimensions of the structure are calculated by considering operating frequency of 6.85 GHz and wavelength of 43.796 mm/s and designed to operate in the spectrum of UWB covering the span of 3.1–10.6 GHz. Over the lower band, the antenna resonates in the fundamental mode; over the upper band, it resonates in the higher order modes. The antenna resonates at four frequencies which are 3.45, 6.675, 8.2, and 10.67 GHz. When generated electromagnetic waves are in-phase, constructive interference is created which results in gain enhancement. The observed peak gain values of simulated and measured structures are 6.734 and 6.635 dB at the frequencies 8.2 GHz and 7.9 GHz, respectively [33]. The antenna structure is fabricated by using a double sided copper flame retardant epoxy glass composite dielectric substrate and tested, and results are validated with the help of model N9916A of vector network analyzer (VNA). The fabricated prototype is depicted in Fig. 2, and the optimized results from simulator as well as measured results from VNA of reflection characteristics and gain variations are in Fig. 3 and Fig. 4, respectively.

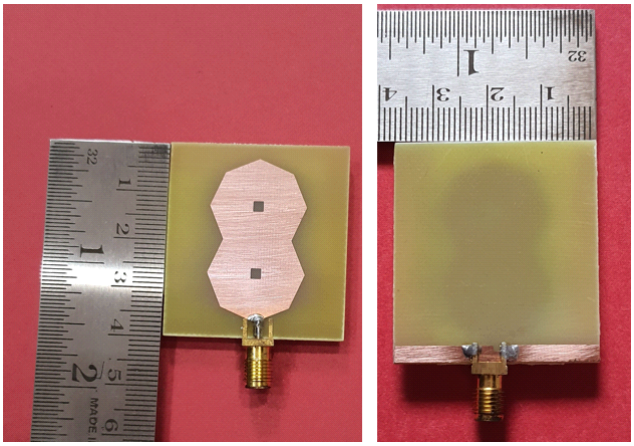

FIGURE 2. Prototype of UWB antenna.

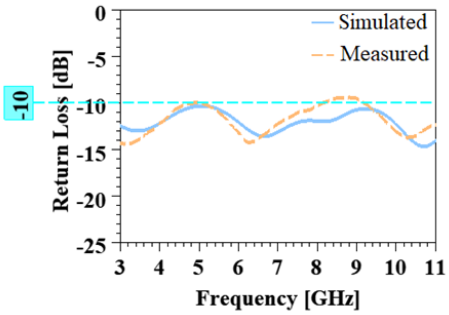

FIGURE 3. Return loss of prototype [33].

4. ANALYSIS OF BREAST MODEL

The impetus of the breast phantom is to replicate all aspects of realistic breast with their appropriate traits. Ultra-precise breast phantoms are essential resources for experimental and computational investigations. Here, by examining the anatomy

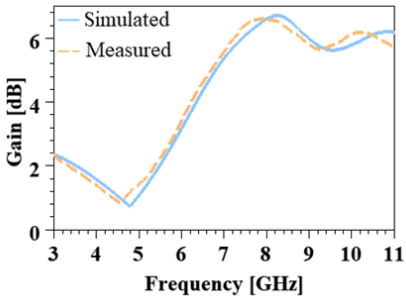

FIGURE 4. Gain variations verses frequency of proposed UWB antenna [33].

of the breast, a phantom that mimics the realistic breast dielectric properties is created. A female breast is composed of different layers: epidermal, adipose, glandular, and tumor tissues that are embedded within. The virtue of identifying lesions in the breast using microwave sensing hinges on dielectric characteristics of the tissue. Breast tissue has diverse contrast levels between healthy and cancerous tissues. The electromagnetic waves emitted from an antenna sensor propagate through different layers of the breast and interact with them. These tissues appear to be lossy dispersive materials when being exposed to electromagnetic waves, which influences the resulting signal through absorption, transmission, and reflections. Debye model is employed to elucidate the alterations in dielectric traits of breast cells as a function of frequencies. Single pole Debye dispersion model is expressed as,

$$\varepsilon_r(\omega) = \varepsilon_\infty + \frac{\varepsilon_s - \varepsilon_\infty}{1 + \omega^2\tau^2} \tag{1}$$

$$\sigma_r(\omega) = \frac{(\varepsilon_s - \varepsilon_\infty)\omega^2\tau\varepsilon_0}{1 + \omega^2\tau^2} + \sigma_s \tag{2}$$

where ε_r — Complex permittivity, ε_0 — Free space permittivity, ε_s — Static dielectic constant, ε_∞ — Dielectric constant at infinity, σ_s — Static conductivity, τ — Pole relaxation constant, ω — Angular frequency.

4.1. Evaluation Framework

The entire system encompassing antenna radiator and breast model is designed using Ansys High Frequency Structure Simulator (HFSS) software. The breast phantom is of two types: homogeneous and heterogeneous ones. The heterogeneous phantom is composed of skin, fatty, glandular, and tumor layers. The outermost skin layer is quite thin, while the fatty and glandular layers account for 50% of the overall thickness. The breast model of different sizes is modelled by using varying thickness as listed in Table 1. The complex permittivity and dielectric constant range 26.2–40 and 0.347–0.636 for skin, 4.25–5.42 and 0.158–0.264 for fat, 36.1–54.3 and 0.28–0.596 for gland, 50–70 and 3–4 for tumor, respectively. Each layer of the breast model is composed by referring the dielectric properties listed in Table 2. The modeled system framework is presented in Fig. 5, which includes the antenna as a sensor and a breast model without and with tumor.

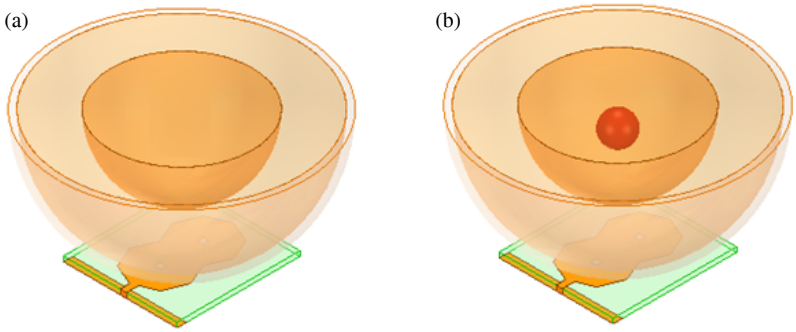

FIGURE 5. Breast phantom modelling in HFSS. (a) Breast model without tumor. (b) Breast model with tumor.

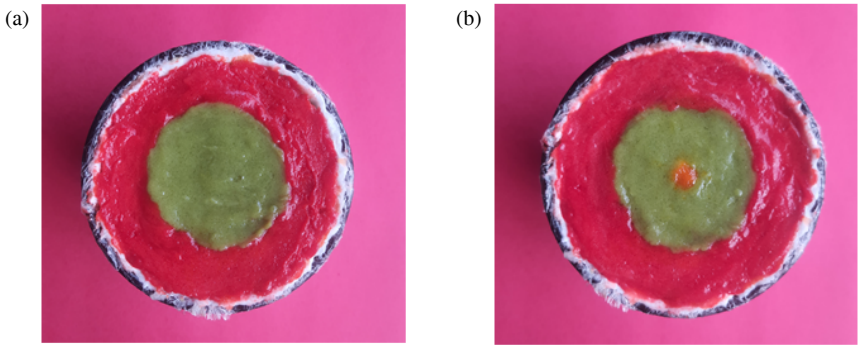

FIGURE 6. Fabrication of breast phantom. (a) Breast phantom without tumor. (b) Breast phantom with tumor.

TABLE 1. Design dimension details of different breast tissues.

Sr. No.	Breast Tissue Type	Breast Thickness (mm)				
		40	50	60	70	80
1	Skin	2	2	2	2	2
2	Fatty	18	23	28	33	38
3	Glandular	20	25	30	35	40
4	Tumor	4, 5, 6, 7				

TABLE 2. Electromagnetic parameters of various breast tissues [9].

Sr. No.	Breast Tissue Type	ε_r	σ_s (S/m)	τ (ps)
1	Skin	35	1.10	7.37
2	Fatty	5	0.262	7.00
3	Glandular	45	0.46	7.00
4	Tumor	64.9	4	7.00

4.2. Fabrication Process

The various procedures are investigated to fabricate the replica of breast tissues [6–9]. The heterogeneous breast phantom of size 80 mm with dimensions mentioned in Table 1 is constructed by using the chemical constituents specified in Table 3. The appropriate combination of chemical materials is used to acquire high permittivity of phantom by using distilled water and low conductivity by propylene glycol and safflower oil. These constituents moreover provide notable mechanical strengths and are simple to synthesize. Even though varying concentrations of these materials are employed to create breast phantom layers, the selected materials make fabrication process easy.

Fabrication Procedure:

1. At the temperature of 80°C, in double boiler heat the mixture of propylene glycol with distilled water.
2. Incorporate agar-agar gelatin powder into the mixture, stir until it liquefies and changes the color. The phantom shape is well-preserved through this incorporation. Notably, this mixture exhibits dielectric properties closely resembling those of realistic breast tissues.
3. Mix liquid detergent and formalin with safflower oil, then combine it with the heated solution. Formalin ensures the stabilization of the phantom.
4. Get the mixture out of the boiler, then mix xanthan gum until it cools off. The combination of liquid detergent, formalin, and xanthan gum acts as a surfactant and thickener.
5. Place the solution in an ice bath and stir it gently.
6. Once the mixture cools to 25°C, pour it into a mold and refrigerated.

The fabricated breast tissues, phantoms without and with tumor are presented in Fig. 6.

TABLE 3. Material and composition for breast phantom fabrication.

Sr. No.	Material	Skin	Fat	Gland	Tumor
1	Distilled Water (ml)	100	50	100	120
2	Propylene Glycol (ml)	7	2	7	7
3	Agar-Agar Gelatin Powder (g)	6	7	5	10
4	Safflower Oil (ml)	14	40	21	9
5	Liquid Detergent (ml)	0.5	0.5	0.5	0.5
6	Formalin (ml)	0.3	0.3	0.3	0.3
7	Xanthan Gum (g)	2.5	2	2	2

4.3. Analysis of Breast Layers

The principle of microwave sensing to detect lesion in the breast relies on dielectric characteristics of the tissue. The effective distinction between tumorous and healthy tissue is made possible by their contrasting characteristics. The system model incorporating antenna sensor and breast model is validated by using a model N9916A of VNA. Ultrasound gel is utilized which serves as the surface matching material to reduce the losses occurring between the sensor and breast model. The five sets of reflection characteristics are recorded in a span of four to five days. The average value of these five sets of recorded samples is taken into account for the subsequent analysis. Fig. 7 presents reflection characteristics as a function of frequency variations of prototype of the breast model without and with tumor. According to analysis, there are prominent deviations in the reflection properties; tumorous tissue exhibited a higher return loss than healthy tissue as depicted in Fig. 7. This change in reflection characteristics is because the lesion in the breast absorbs more electromagnetic energy. Thus, malignant tissues manifest themselves as scattering materials with significant losses for microwave propagation, which leads to the phenomenon that the return loss from the tumor layer is remarkably higher. Further, the dielectric properties are extracted by using Equations (1) and (2) from the analyzed data. The reflection and dielectric characteristics of different breast layers are shown in Fig. 8.

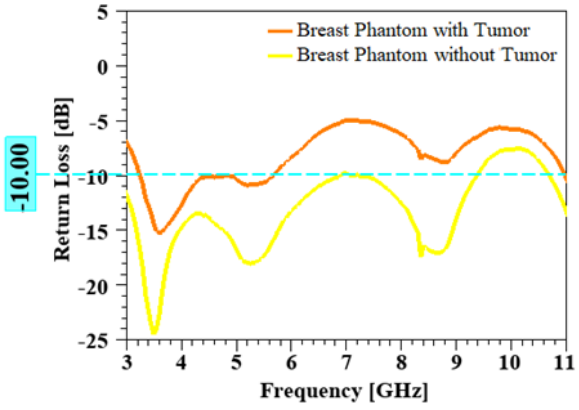

FIGURE 7. Reflection characteristics of breast model without and with tumor.

Specific absorption rate (SAR) essentially serves as a metric to quantify the amount of energy or heat that can be produced in a specific volume of human tissue as a result of energy absorption from an electromagnetic field that a device emits. For a given mass density ρ, as per the Institute of Electrical and Electronics Engineers (IEEE), the Specific Absorption Rate (SAR) is defined as the time derivative of the incremental energy (dW) absorbed by an incremental mass (dm) contained in a volume element (dV). Specific absorption power density (SAPD) is a unit of non-ionizing radiation, inversely proportional to electromagnetic wave frequency and square of electric field vector causing bio effects. SAR is given by:

$$SAR = \frac{d}{dt}\left(\frac{dW}{dm}\right) = \frac{d}{dt}\left(\frac{dW}{\rho dV}\right) \tag{3}$$

$$SAR = \frac{\sigma|E|^2}{\rho} \tag{4}$$

where SAR — Specific Absorption Rate (W/kg), σ — conductivity (S/m), ρ — the mass density (kg/m^3).

The limits of controlled and uncontrolled environments for SAR over whole-body SAR of tissue 1 g and 10 g are listed in Table 4.

TABLE 4. Specific absorption rate.

Environment	SAR		
	Whole-Body	1 g	10 g
Controlled	0.4	8	20
Uncontrolled	0.08	1.6	4

This section illustrates the importance of using SAR value coordinates to locating a breast tumor. SAR is the most important key aspect that should be considered as it is a measure of safety for patients. The incident microwaves get more absorbed by the tumorous tissues than normal tissues. The absorption of EM waves is measured as SAR and can be a useful tool for the identification of the presence of malignant tissues and location of the tumor within the tissues. The mere fact that the two breasts of a female are identical to each other eases identifying the existence of a tumor. Here, a breast model is analyzed using Ansys HFSS software to examine the SAR study. A

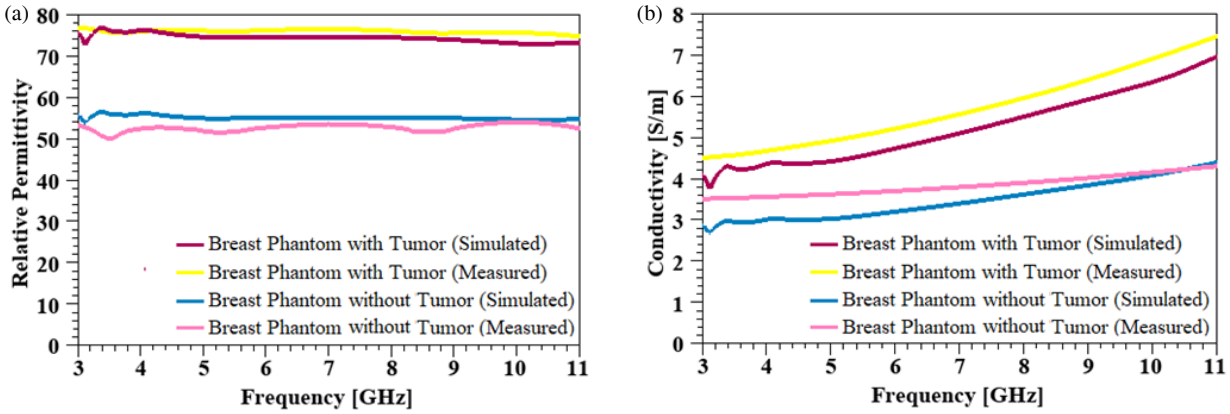

FIGURE 8. Dielectric properties of different breast tissue types. (a) Relative permittivity. (b) Conductivity.

TABLE 5. Specific absorption rate (W/Kg) for varying sizes of simulated breast models.

Frequency (GHz) \ Breast Size (mm)	40		50		60		70		80	
	Without Tumor	With Tumor	Without Tumor	With Tumor	Without Tumor	With Tumor	Without Tumor	With Tumor	Without Tumor	With Tumor
3	1.574	8.072	1.685	9.768	1.795	12.652	1.807	19.888	1.908	28.987
4	0.176	2.305	1.385	3.381	0.250	1.899	1.639	13.737	1.324	11.55
5	0.135	1.140	1.561	5.403	0.066	0.488	0.216	2.549	0.222	0.384
6	0.021	0.185	0.090	0.425	0.0076	0.034	0.023	0.222	0.039	0.084
7	0.0084	0.074	0.027	0.196	0.0031	0.0103	0.013	0.073	0.020	0.041
8	0.0092	0.092	0.027	0.135	0.0022	0.0051	0.0077	0.035	0.012	0.021
9	0.011	0.123	0.018	0.095	0.0018	0.0033	0.0049	0.021	0.006	0.0089
10	0.012	0.119	0.017	0.062	0.0013	0.0021	0.0046	0.018	0.002	0.0037

breast model varying in size from 40 mm to 80 mm is employed to examine SAR values. The two phantoms without and with tumor of size 5 mm are utilized to measure the SAR values. Table 5 summarizes the disparities between the two scenarios. The SAR value becomes higher with tumor since the lesion absorbs even more electromagnetic energy than healthy tissues. Furthermore, the SAR values are examined by varying tumor size from 7 to 4 mm. It is noted that the SAR values increase in tandem with the growth of the tumorous cells. The position of the lesion is determined by the (x, y, z) coordinates of maximal SAR values. Table 6 displays the true position of the embedded tumor and the location of the lesion as estimated by inspecting at the maximal SAR values for different tumor sizes. Fig. 9(a) shows the simulated SAR value of the healthy breast. As depicted in Figs. 9(b)-(f), a 5 mm tumor is embedded in the mammary gland at different positions, the top, bottom, left, and center, for analyzing the SAR values by simulation.

5. DATA ANALYSIS AND CLASSIFICATION ALGORITHMS

An AI-derived method for intelligent decision-making in automated systems is machine learning. A descriptive learning approach called unsupervised learning and predictive approach as supervised learning are its two primary categories. A classification method is a systematic approach to construct a classifier from an input data set, based on a learning target function that maps each feature set to a predefined label of the class, particularly effective for predicting or characterizing binary or nominal datasets. Unsupervised learning is perfect for exploratory data analysis, cross-selling strategies, segmentation and recognition since it leverages machine learning techniques to analyze and cluster unlabeled information and reveal underlying links or patterns without the need of human intervention. There are two techniques for reducing dimensionality: feature selection, which entails retaining just the most pertinent features from the

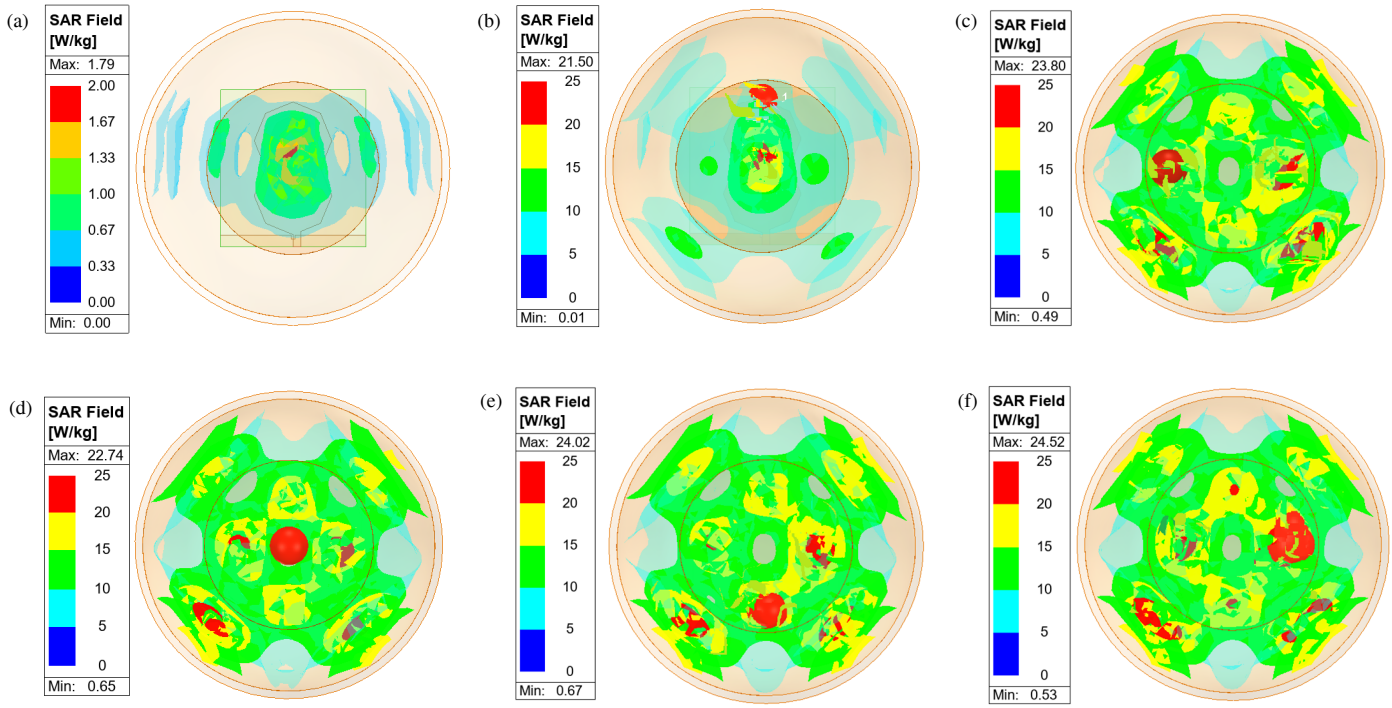

FIGURE 9. Simulated SAR field of tumor of size 5 mm for varying position. (a) No tumor, (b) Top (0, 16, 33), (c) Left (−16, 0, 33), (d) Center (0, 0, 32), (e) Bottom (0, −16, 33), (f) Right (16, 0, 33).

TABLE 6. Identification of tumor position for different tumor dimensions.

Embedded Tumor Size (mm)	Embedded Tumor Location (x,y,z) co-ordinates (mm)		Embedded Tumor Size (mm)	Embedded Tumor Location (x,y,z) co-ordinates (mm)	
	Embedded	At max average SAR		Embedded	At max average SAR
7	0, 0, 30	0, 0, 29.59	6	0, 0, 30	0, 0, 30.59
	2.5, 0, 30	2.44, 0.31, 28.59		−5.2, 0, 30	−5.23, −2.1, 29.59
	2, 2, 30	2, 2.03, 30.59		4.5, 4.5, 30	4.6, 4.5, 30.79
	2, −2, 30	1.98, −2, 28.59		0, −6, 30	0.9, −6, 29.59
5	0, 0, 32	0, 0, 31.59	4	0, 0, 33	0, 0, 32.79
	−5.5, 6, 32	−5.43, 6.76, 31.59		0, 10, 33	0, 9.8, 32.79
	5.8, −5.8, 32	4.8, −5.77, 30.59		7, −7, 33	6.17, −7.05, 31.79
	−5.5, −5.5, 32	−5.57, −4.91, 31.59		−7, −7, 33	−6, −5.94, 32.59

original dataset, and feature extraction, which looks at the interdependencies of the original dataset by identifying a smaller set of new features. The data visualization of dielectric traits of different layers of the breast on recorded dataset is depicted in Fig. 10. Data visualization before reducing dimensionality is presented in Fig. 11.

5.1. Principal Component Analysis (PCA)

The most ancient yet highly adaptable statistical method in multivariate analysis is PCA that extracts significant information from a dataset containing inter-correlated quantitative dependent variables. The key objective of a PCA analysis is to extract crucial data from a dataset, reduce its size, streamline its description, and examine its structure. It creates principal components, representing the table as a collection of new orthogonal variables, and displays patterns of similarity between variables and observations as points in mapping. PCA is contingent on the eigen-decomposition and singular value decomposition. Principal Component Analysis can be probabilistically reformulated by extracting the principal sub-space of observed data using a generative latent variable model with maximum likelihood solution. The PCA algorithm is summarized as follows:

1. Data Conditioning: Normalize each feature.
2. Construct covariance matrix: Prepare a square matrix to illustrate the relationship between the features. The covariance matrix is expressed as:

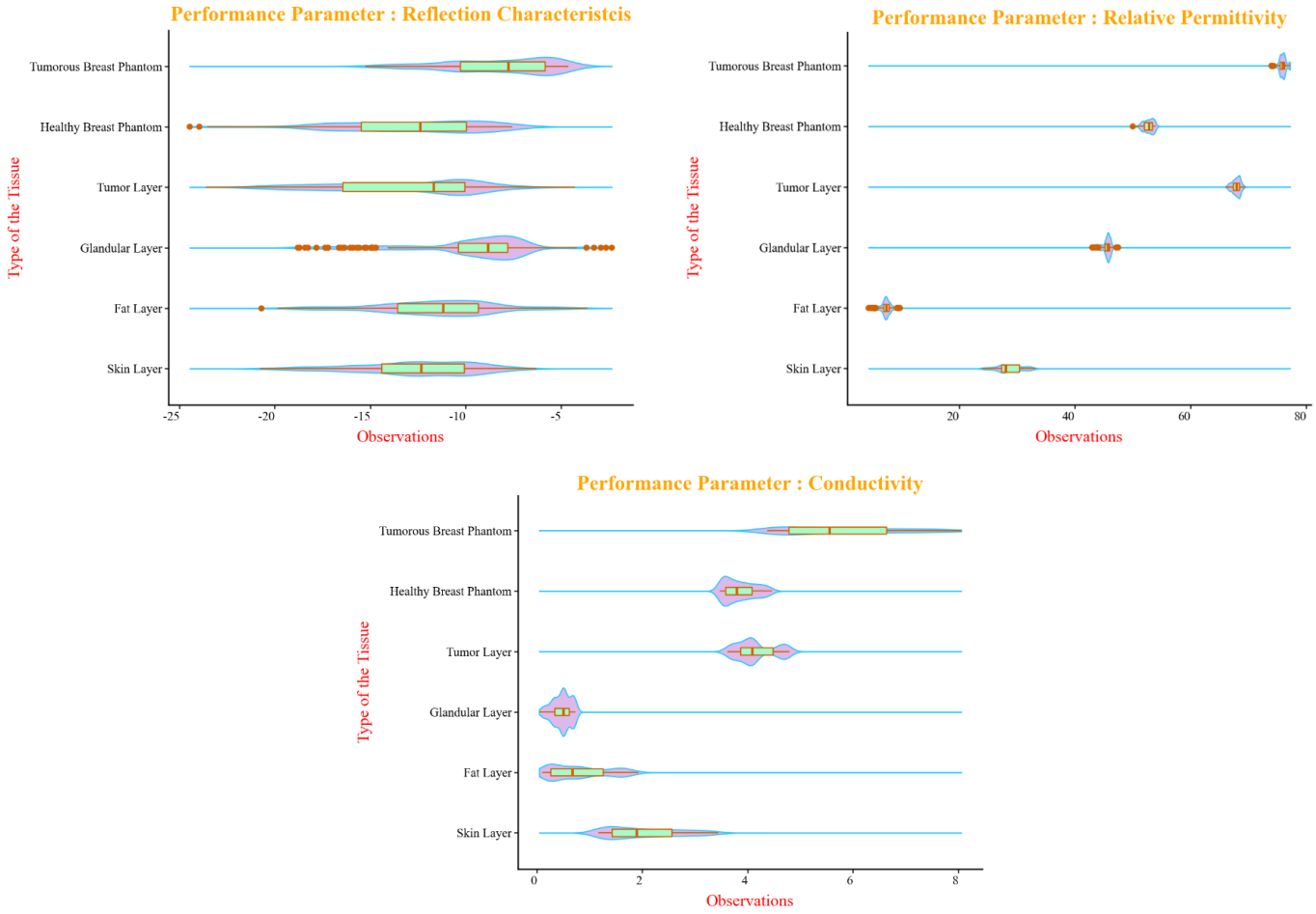

FIGURE 10. Data visualization of dielectric traits for different breast tissues.

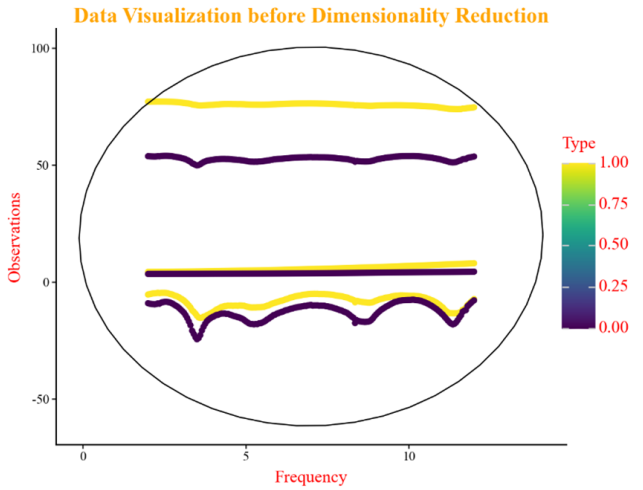

FIGURE 11. Data Visualization of dielectric traits of breast phantom before dimensionality reduction.

$$Cov(A_i, A_j) = \frac{\sum_{k=1}^{n} (A_{ik} - \sum A_i)(A_{jk} - \sum A_j)}{n-1} \quad (5)$$

where $Cov(A_i, A_j)$ — signify the covariance between the dataset's attribute A_i and A_j across n observations, A_i and A_j — arithmetic of variables A_i and A_j.

1. Compute the eigenvalues and eigenvectors concomitant to the covariance matrix.
2. Order the eigenvectors from top to bottom by selecting the most significant ones and disregarding the least ones.

Here, PCA is applied on the recorded dataset, and three principle components are extracted. The extracted features are shown in Fig. 12. After applying transformation and fitting the model, obtained PCA components are: [[1.00, 2.42e-10, 0.0], [-2.42e-10, 1.00, 0.0], [0.0, 0.0, 1.00]]. The supervised machine learning techniques including support vector machine (SVM), multilayer perceptron (MLP), K-nearest neighbor (KNN), and random forest (RF) are implemented to classify the presence of breast tumor. Among them, random forest provides the best fit with auc score of 0.9960.

5.2. t-Distributed Stochastic Neighbor Embedding (tSNE)

An unsupervised nonlinear dimensionality reduction technique for high-dimensional data representation and data exploration is tSNE. The algorithm reduces dimensions in a nonlinear way, helping to separate complex structures that cannot be represented by a straight line. tSNE applies a balanced cost function, easier to compute gradients and student-t distribution to evaluate the similitude between two points in the lower-dimensional

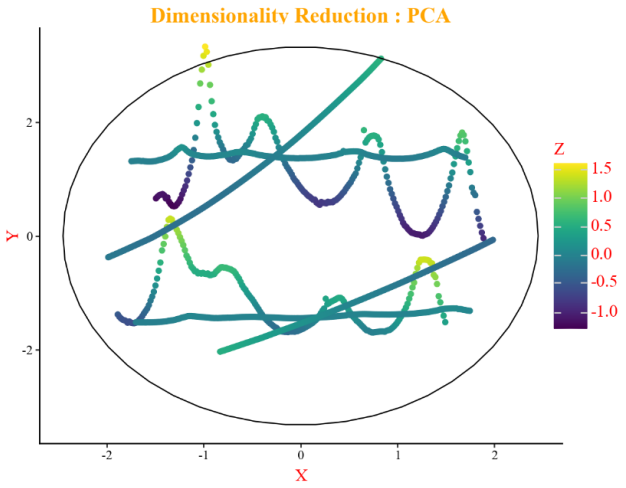

FIGURE 12. Data visualization of dielectric traits after PCA dimensionality reduction technique.

space. tSNE begins by transforming high-dimensional Euclidean distances into conditional probabilities to signify point similarities. A common way to assess the correctness of conditional probabilities is through Kullback-Leibler (KL) divergence. The KL divergence is equivalent to the cross-entropy with a control variable. The summation of Kullback-Leibler divergences is reduced by SNE across all data points through gradient descent. The cost function C of tSNE is expressed as,

$$C = KL(PallelQ) = \sum_i \sum_j p_{ij} \log \frac{p_{ij}}{q_{ij}} \quad (6)$$

$$p_{ij} = \frac{\exp(-\|x_i - x_j\|^2/2\sigma^2)}{\sum_{k \neq l} \exp(-\|x_k - x_l\|^2/\sigma^2)} \quad (7)$$

$$q_{ij} = \frac{\exp(-\|y_i - y_j\|^2)}{\sum_{k \neq l} \exp(-\|y_k - y_l\|^2)} \quad (8)$$

$$\frac{\delta C}{\delta y_i} = 4 \sum_j \frac{(p_{ij} - q_{ij})(y_i - y_j)}{(1 + \|y_i - y_j\|^2)} \quad (9)$$

where P_i — conditional probabilities for each data point in relation to x_i, Q_i — conditional probabilities for each data point in relation to y_i, σ^2 — variance.

The goal is to minimize a single KL divergence loss between high and low dimensional spaces. The similarity measurement between pairs of instances in higher and lower dimensions' spaces is found by tSNE method. The algorithm employs a probabilistic model to measure point similarities, using a Gaussian distribution for higher dimensions and a student's t-distribution for lower dimensions. It then tries to maximize two similarity metrics. The algorithm embeds data into lower dimensions as follows:

1. tSNE simulates the process of choosing the points in both upper and lower dimensions as a neighbour of another point. It initially employs a Gaussian kernel to compute pairwise similarities in high-dimensional space, assigning lower selection probabilities to distant points than to nearby ones.
2. Subsequent to this, retaining pairwise similarities, the algorithm tries to transfer high-dimensional data samples into lower space.
3. Minimizing the divergence between the original high-dimensional and lower-dimensional probability distributions is how it is accomplished. To reduce the divergence, the technique employs gradient descent. The lower-dimensional representation converges to an optimal state.

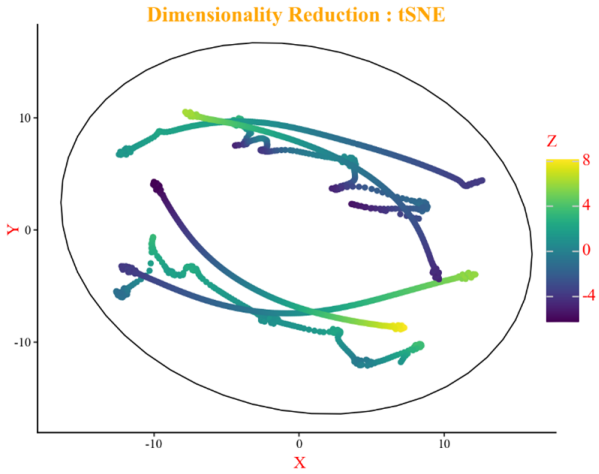

FIGURE 13. Data visualization of dielectric traits after tSNE dimensionality reduction technique.

Through the process of optimization, related data points may be grouped and sub-grouped in the low level space, which can then be visualized to help comprehend the structure and relationships found in the higher-dimensional data. The tSNE model is applied on the recorded dataset with three dimension of the embedded space. The Kullback-Leibler divergence obtained after transforming the recorded dataset into embedded space and fitting the model is: $[-0.03478, 0.0323]$. The reduced dimensionality of the dataset is presented in Fig. 13. Further, the data obtained from tSNE model is processed by supervised learning models, KNN, SVM, RF, and MLP to predict the existence of the breast tumor. The models are optimized by hyper tuning the parameters to enhance the detection accuracy. Table 7 briefs about the performance of these algorithms.

TABLE 7. Performance metric.

Sr. No	Algorith	F1 Score	AUC Scor
1	Support Vector Machine	0.9838	0.9917
2	Multilayer Perceptro	0.9138	0.9520
3	K-Nearest Neighbor	0.9636	0.9752
4	Random Fores	0.9876	0.9997

6. COMPARISON WITH LITERATURE

The proposed integrated octagon-shaped microstrip patch antenna structure is intended for UWB frequency spectrum and

TABLE 8. Analysis in relation to previous work.

Ref. No.	System Outline	Dataset	Algorithm	Performance Metric (Accuracy/AUC)
[22]	Breast Cancer Diagnosis by Experimental Comparison of Classifiers	WBC	NB	95.99%
		WDBC	NB	96.66%
		WBC	J48	95.13%
		WDBC	SMO	97.71%
		WDBC	IBK	95.95%
[23]	Clustering using K-Means and Dimensionality Reduction using PCA for Breast Cancer Prediction	WBC	PCA, KNN, SVM	97.66%
			PCA, KNN, XGBOOST	97.66%
[25]	10-fold cross validation using MLP, Transfer Learning, and SVM for Breast Cancer Detection System	Manuel Gomes (University Hospital Centre of Coimbra)	PCA, MLP, SVM	86.94%
[26]	The medical CAD categorization system through k-fold cross-validation using ANN, KNN, SVM, DT, RF, XGboost, and Adaboost with S-LR classifier for breast cancer disease prediction	WBCD	S-LR	97.37%
		Mammographic Mass	S-LR	93.37%
[27]	UWB-RMSA for Breast Cancer Detection using microwave sensing 20.47 × 10.56 No. of sensors: 2	UWB RMSA Prototype	RF	94.4%
[28]	Vivaldi antenna with circular holographic for microwave imaging 56 × 56 No. of sensors: 2	UWB transceivers Prototype	LDA	87.10%
			QDA	89.29%
[29]	Multi-static Radar System operated in Time-Domain for Microwave Breast Screening No. of sensors: 16 element arrays (2 switching matrix)	UWB Prototype	LDA	70.30%
			SVM	73.64%
[30]	Ultra wide-band transceivers for detection of breast tumor using neural networks. No. of sensors: 2	UWB transceivers antenna setup	NN trainscg	94.42%
			NN traingdm	88.42%
[31]	Dual port wearable textile MIMO CPW-fed UWB antenna and use of machine learning for the detection of breast cancer. 60 × 70 No. of sensors: 1	UWB MIMO Prototype	RF	85%
			SVM	99%
PA	Integrated Octagonal Microstrip Antenna for breast tumor detection 40 × 40 No. of sensors: 1	UWB MI-OMSA Prototype	tSNE, SVM	99.17%
			tSNE, MLP	95.20%
			tSNE, KNN	97.52%
			tSNE, RF	99.97%

to analyze the dielectric traits of different layers of the breast model. Breast tumor detection accuracy is improved by implementing machine learning algorithms. Thereby, the antenna structure is compared with the UWB antennas used for the application of breast tumor detection in the literature with respect to the size of antenna, number of sensors, dataset, algorithms, and detection accuracy with accuracy score. This comparison is listed in Table 8.

7. CONCLUSION

This study has examined the performance of an ultra-wideband antenna in breast phantom layers, focused on simulation and evaluation of the interaction of electromagnetic waves with various tissue-like phantom layers, including skin, fatty, glandular, and tumorous tissues, which serve as analogs to human breast anatomy. A UWB antenna along with breast phantom is modelled using high-frequency structure simulator software, fabricated and tested using vector network analyzer model N9916A. It is evident that aberrant cell absorbs more electromagnetic energy than healthiest one. It is because inherent electrical properties of breast tissues make them appear to be lossy dispersive materials at microwave propagation, which raises the value of reflection characteristics of tumor-layered phantoms relative to those of healthy breast phantoms. SAR field is useful for examining the maximum absorbed energy in the breast tissues. The tumor of varying sizes from 7 mm to 4 mm is embedded into mammary gland layer of breast model, and location is identified at maximum average SAR value. The data is recorded by testing antenna structure along with breast phantoms with and without tumors, using ultrasound gel as a matching medium. The exploratory data analysis is performed by using dimensionality reduction techniques for feature extractions. PCA and tSNE algorithms are used to select the principle components from highly dimensional recorded data. The supervised algorithms are applied to the extracted features and used to categorized tissues as healthy or tumorous. The auc score is used as performance metric to assess the model. The auc score obtained by SVM, MLP, KNN, and RF with tSNE as dimensionality reduction technique is 99.17%, 95.20%, 97.52%, and 99.97%, respectively. The highest auc score among the mentioned algorithms is obtained by the combination of RF algorithm of 99.97% and hence proven to be the best fit on the recorded dataset to improve the detection accuracy. The research suggests that UWB antennas can improve early breast cancer detection and enhance microwave sensing accuracy by integrating ML techniques, contributing to more effective breast cancer screening techniques.

REFERENCES

[1] Giaquinto, A. N., H. Sung, L. A. Newman, R. A. Freedman, R. A. Smith, J. Star, A. Jemal, and R. L. Siegel, "Breast cancer statistics 2024," *CA: A Cancer Journal for Clinicians*, Vol. 74, No. 6, 477–495, 2024.

[2] García-Figueiras, R., S. Baleato-González, A. R. Padhani, A. Luna-Alcalá, J. A. Vallejo-Casas, E. Sala, J. C. Vilanova, D.-M. Koh, M. Herranz-Carnero, and H. A. Vargas, "How clinical imaging can assess cancer biology," *Insights into Imaging*, Vol. 10, No. 1, 28, 2019.

[3] Heywang-Köbrunner, S. H., A. Hacker, and S. Sedlacek, "Advantages and disadvantages of mammography screening," *Breast Care*, Vol. 6, No. 3, 199–207, 2011.

[4] Fear, E. C., P. M. Meaney, and M. A. Stuchly, "Microwaves for breast cancer detection?" *IEEE Potentials*, Vol. 22, No. 1, 12–18, 2003.

[5] Federal Communication Commission, "First report and order, revision of part 15 of the commissions rule regarding ultra-wideband transmission systems," Technical Report, Washington, DC, Apr. 2002.

[6] Lazebnik, M., E. L. Madsen, G. R. Frank, and S. C. Hagness, "Tissue-mimicking phantom materials for narrowband and ultra-wideband microwave applications," *Physics in Medicine & Biology*, Vol. 50, No. 18, 4245, 2005.

[7] Zhang, H., S. Y. Tan, and H. S. Tan, "A novel method for microwave breast cancer detection," in *2008 Asia-Pacific Microwave Conference*, 1–4, Hong Kong, China, 2008.

[8] Porter, E., J. Fakhoury, R. Oprisor, M. Coates, and M. Popović, "Improved tissue phantoms for experimental validation of microwave breast cancer detection," in *Proceedings of the Fourth European Conference on Antennas and Propagation*, 1–5, Barcelona, Spain, 2010.

[9] Islam, M. T., M. Samsuzzaman, S. Kibria, and M. T. Islam, "Experimental breast phantoms for estimation of breast tumor using microwave imaging systems," *IEEE Access*, Vol. 6, 78 587–78 597, 2018.

[10] El Vadel, L. A., D. B. O. Konditi, and F. M. Mbango, "A miniaturized antenna for breast cancer detection at the 5.72–5.82 GHz ISM band based on the DGS technique," *Progress In Electromagnetics Research B*, Vol. 98, 87–105, 2023.

[11] Hammouch, N., A. Rghioui, H. Ammor, M. Oubrek, and J. Lloret, "A low-cost UWB microwave imaging system for early-stage breast cancer detection," *Multimedia Tools and Applications*, Vol. 84, No. 17, 17 329–17 360, 2025.

[12] Ponnapalli, V. L. N. P., S. Karthikeyan, and J. L. Narayana, "A circular slotted shaped UWB monopole antenna for breast cancer detection," *Progress In Electromagnetics Research Letters*, Vol. 104, 57–65, 2022.

[13] Kahar, M., A. Ray, D. Sarkar, and P. P. Sarkar, "An UWB microstrip monopole antenna for breast tumor detection," *Microwave and Optical Technology Letters*, Vol. 57, No. 1, 49–54, 2015.

[14] Oloumi, D., P. Boulanger, A. Kordzadeh, and K. Rambabu, "Breast tumor detection using UWB circular-SAR tomographic microwave imaging," in *2015 37th Annual International Conference of the IEEE Engineering in Medicine and Biology Society (EMBC)*, 7063–7066, Milan, Italy, 2015.

[15] Dagheyan, A. G., A. Molaei, R. Obermeier, and J. Martinez-Lorenzo, "Preliminary imaging results and SAR analysis of a microwave imaging system for early breast cancer detection," in *2016 38th Annual International Conference of the IEEE Engineering in Medicine and Biology Society (EMBC)*, 1066–1069, Orlando, FL, USA, 2016.

[16] Selvaraj, V. and P. Srinivasan, "Interaction of an EM wave with the breast tissue in a microwave imaging technique using an ultra-wideband antenna," *Biomedical Research*, Vol. 28, No. 3, 1025–1030, 2017.

[17] Subramanian, S., B. Sundarambal, and D. Nirmal, "Investigation on simulation-based specific absorption rate in ultra-wideband antenna for breast cancer detection," *IEEE Sensors Journal*, Vol. 18, No. 24, 10 002–10 009, 2018.

[18] Amdaouch, I., O. Aghzout, A. Naghar, A. V. Alejos, and F. J. Falcone, "Breast tumor detection system based on a compact UWB antenna design," *Progress In Electromagnetics Research M*, Vol. 64, 123–133, 2018.

[19] Abdi, H. and L. J. Williams, "Principal component analysis," *Wiley Interdisciplinary Reviews: Computational Statistics*, Vol. 2, No. 4, 433–459, 2010.

[20] Vander Maaten, L. and G. Hinton, "Visualizing data using t-SNE," *Journal of Machine Learning Research*, Vol. 9, 2579–2605, 2008.

[21] Ak, M. F., "A comparative analysis of breast cancer detection and diagnosis using data visualization and machine learning applications," *Healthcare*, Vol. 8, No. 2, 111, 2020.

[22] Salama, G. I., M. B. Abdelhalim, and M. A.-E. Zeid, "Experimental comparison of classifiers for breast cancer diagnosis," in *2012 Seventh International Conference on Computer Engineering & Systems (ICCES)*, 180–185, Cairo, Egypt, 2012.

[23] Jamal, A., A. Handayani, A. A. Septiandri, E. Ripmiatin, and Y. Effendi, "Dimensionality reduction using PCA and K-means clustering for breast cancer prediction," *Lontar Komputer : Jurnal Ilmiah Teknologi Informasi*, Vol. 9, No. 3, 192–201, 2018.

[24] Mushtaq, Z., A. Yaqub, A. Hassan, and S. F. Su, "Performance analysis of supervised classifiers using PCA based techniques on breast cancer," in *2019 International Conference on Engineering and Emerging Technologies (ICEET)*, 1–6, Lahore, Pakistan, Feb. 2019.

[25] Chiu, H.-J., T.-H. S. Li, and P.-H. Kuo, "Breast cancer–detection system using PCA, multilayer perceptron, transfer learning, and support vector machine," *IEEE Access*, Vol. 8, 204 309–204 324, 2020.

[26] Laghmati, S., S. Hamida, K. Hicham, B. Cherradi, and A. Tmiri, "An improved breast cancer disease prediction system using ML and PCA," *Multimedia Tools and Applications*, Vol. 83, No. 11, 33 785–33 821, 2024.

[27] AlShehri, S. A., S. Khatun, A. B. Jantan, R. S. A. R. Abdullah, R. Mahmud, and Z. Awang, "3D experimental detection and discrimination of malignant and benign breast tumor using NN-based UWB imaging system," *Progress In Electromagnetics Research*, Vol. 116, 221–237, 2011.

[28] Conceição, R. C., H. Medeiros, M. O'Halloran, D. Rodriguez-Herrera, D. Flores-Tapia, and S. Pistorius, "Initial classification of breast tumour phantoms using a UWB radar prototype," in *2013 International Conference on Electromagnetics in Advanced Applications (ICEAA)*, 720–723, Turin, Italy, 2013.

[29] Santorelli, A., E. Porter, E. Kirshin, Y. J. Liu, and M. Popović, "Investigation of classifiers for tumor detection with an experimental time-domain breast screening system," *Progress In Electromagnetics Research*, Vol. 144, 45–57, 2014.

[30] Aydin, E. A. and M. K. Keleş, "UWB rectangular microstrip patch antenna design in matching liquid and evaluating the classification accuracy in data mining using random forest algorithm for breast cancer detection with microwave," *Journal of Electrical Engineering & Technology*, Vol. 14, No. 5, 2127–2136, 2019.

[31] Elnaggar, A. H., A. S. A. El-Hameed, M. A. Yakout, and N. F. F. Areed, "Machine learning for breast cancer detection with dual-port textile UWB MIMO bra-tenna system," *Information*, Vol. 15, No. 8, 467, 2024.

[32] Kamil, R. A., N. T. Mahmood, Z. S. Muqdad, M. H. Jwair, N. M. Noori, and T. A. Elwi, "On the performance of metasurface Vivaldi antenna in breast Cancer detection using artificial neural networks for Bio-signal analysis," *Progress In Electromagnetics Research B*, Vol. 111, 31–43, 2025.

[33] Patil, S. and A. Naik, "Design of microstrip antenna by integrating octagonal patch configuration for UWB application," *Advanced Electromagnetics*, Vol. 14, No. 2, 45–56, Jun. 2025.